Optimization of process parameters of Nd:YAG laser microgrooving of Al_2TiO_5 ceramic material by response surface methodology and artificial neural network algorithm

D Dhupal, B Doloi, and **B Bhattacharyya***
Department of Production Engineering, Jadavpur University, Kolkata, India

The manuscript was received on 5 January 2007 and was accepted after revision for publication on 25 April 2007.

DOI: 10.1243/09544054JEM814

Abstract: The high-intensity pulsed Nd:YAG laser has the capability to produce both deep grooves and microgrooves on a wide range of engineering materials such as ceramics, composites, and diamond. The micromachining of ceramics is highly demanded in industry because of its wide and potential uses in various fields such as automobile, electronic, aerospace, and biomedical engineering. Engineering ceramic, i.e. aluminium titanate (Al_2TiO_5), has tremendous application in the automobile and aero-engine industries owing to its excellent thermal properties. The present paper deals with the artificial neural network (ANN) and response surface methodology (RSM) based mathematical modelling and also an optimization analysis of the machining characteristics of the pulsed Nd:YAG laser during the microgrooving operation on Al_2TiO_5. The experiments were planned and carried out based on design of experiments (DOE). Lamp current, pulse frequency, pulse width, assist air pressure, and cutting speed were considered as machining process parameters during the pulsed Nd:YAG laser microgrooving operation and these parameters were also utilized to develop the ANN predictive model. The response criteria selected for optimization were upper width, lower width, and depth of the trapezoidal microgroove. The optimal process parameter settings were obtained as an assist air pressure of 1.2944 kgf/cm^2, lamp current of 19.3070 A, pulse frequency of 1.755 kHz, pulse width of 5.7087 per cent of duty cycle, and cutting speed of 10 mm/s for achieving the desired upper width, lower width, and depth of the laser microgroove. The output of the RSM optimal data was validated through experimentation and the ANN predictive model. A good agreement is observed between the results based on the ANN predictive model and the actual experimental observations.

Keywords: pulsed Nd:YAG laser, microgrooving, artificial neural networks, design of experiments, response surface methodology, Al_2TiO_5

1 INTRODUCTION

With the rapid advance in material machining technology, the applications of engineering ceramic in the micromanufacturing and microfabrication industry are increasing daily. Engineering ceramic, i.e. aluminium titanate (Al_2TiO_5), has superior properties such as low coefficient of friction, good wear and corrosion resistance, low thermal conductivity, relatively high thermal expansion coefficient, good thermal shock resistance, and high fracture toughness [**1**]. The main concern of the manufacturing industry is the machining of difficult-to-process materials and advanced ceramics such as Al_2TiO_5 with high accuracy and faster rate, and laser machining is a promising non-contact machining process for the effective machining of such materials [**2**]. Increasing interest in the use of lasers for manufacturing can be attributed to several unique advantages that are generally applicable to the entire range of materials processing applications, such as high productivity, non-contact processing, elimination of finishing operations, adaptability to automation, reduced

**Corresponding author: Department of Production Engineering, Jadavpur University, Kolkata, West Bengal, 700032, India. email: bijoy_b@sify.com*

processing cost, improved product quality, greater material utilization, minimal heat-affected zone (HAZ), and green manufacturing [**3**, **4**].

In practical applications such as drilling, cutting, or scribing, it is necessary to find a set of laser parameters that provides the desired results under particular processing constraints [**5**]. The laser–material interactions play a significant role in forming the surface profile and resultant geometry of the machined microgroove [**6**]. The assist air pressure has a great effect on the depth and kerf width of the machined groove [**7**]. The laser parameters typically include pulse energy, repetition rate, feed rate, spot size, and pulse duration [**8**]. The typical constraints encountered with ceramic materials include the properties of the ceramic, the desired feature quality and size, and the thermal properties [**9**]. There is a need for precise control of a large number of laser parameters with random components, which makes the task of improving machining performance very difficult. In order to achieve a higher-quality machined surface and better accuracy during laser microgrooving on hard engineering ceramics, especially Al_2TiO_5, intensive research is needed.

In multiple-pulse laser machining, the upper width of the groove is normally larger than required and thus control of the upper width of the machined microgroove is difficult. The lower width and depth generation by the Nd:YAG laser depends on the parametric combination of the laser beam. Also, non-uniform melting and ejection of material from the groove walls and laser power reduction, as the beam propagates into the groove, can be identified as causes for the variation in lower width and depth [**10**, **11**]. An artificial neural network (ANN) approach is an effective tool to predict process parameters; it can generate the outputs for a set of inputs that are within the range of the original inputs during the training phase [**12**]. In the present work, a combination of response surface optimization and ANN modelling was developed for prediction of the precise output of pulsed Nd:YAG laser microgrooving of Al_2TiO_5. In addition, the micromachining of grooves on Al_2TiO_5 by the Nd:YAG laser beam was studied experimentally based on response surface methodology (RSM). The ANN-based predictive model is developed with an emphasis on the characterization of the trapezoidal groove geometry.

2 DETAILS OF THE Nd:YAG LASER MACHINING SYSTEM FOR MICROGROOVING OPERATIONS

The computer numeric control (CNC) pulsed Nd:YAG laser machining system for micromachining operations consists of various subsystems, such as a laser source and beam delivery unit, a power supply unit, a radio-frequency (RF) Q-switch driver unit, a cooling unit, and a CNC controller for *X*-, *Y*-, and *Z*-axes movement. The beam delivery system consists of laser head, RF Q-switch, safety shutter, beam expander, and front and back mirrors. The laser head consists of an Nd:YAG rod and a krypton arc lamp, which are placed in two different focal points of an elliptical cavity. The lasing medium in Nd:YAG lasers is neodymium atoms embedded in an yttrium–aluminium–garnet crystal host. The pump source is usually a krypton arc lamp, which excites the Nd:YAG crystal. For amplification of light, optical feedback is provided by the rear mirror of 100 per cent reflectivity and the front mirror of 80 per cent reflectivity. The Q-switching is an excellent method to produce a very short pulse width and a very high peak power of laser light from a continuous-wave low-power laser. The RF Q-switch driver unit supplies an RF signal to the Q-switch for its operation.

Using the beam delivery system, the laser is focused on to the work spot. The CNC controller consists of *X*–*Y*–*Z* axes and a controlling unit named accupos. Stepper motors are attached to each axis and connected to the accupos. This accupos unit can control the axis movement via computer. The main power supply unit controls the laser output by controlling the current supplied to the krypton arc lamp. The cooling unit cools the system to avoid thermal damage of the laser cavity, lamp, Nd:YAG rod, and Q-switch. Figure 1 is a schematic representation of the CNC Nd:YAG laser machining system. The CNC *Z*-axis controller unit controls the *Z*-axis movement of the lens. A fixture developed to hold a small workpiece of desired shape is mounted over the machining table. A charge-coupled device camera together with a closed-circuit television monitor is used for viewing the location of the workpiece and also for checking the proper focusing condition of the workpiece surface

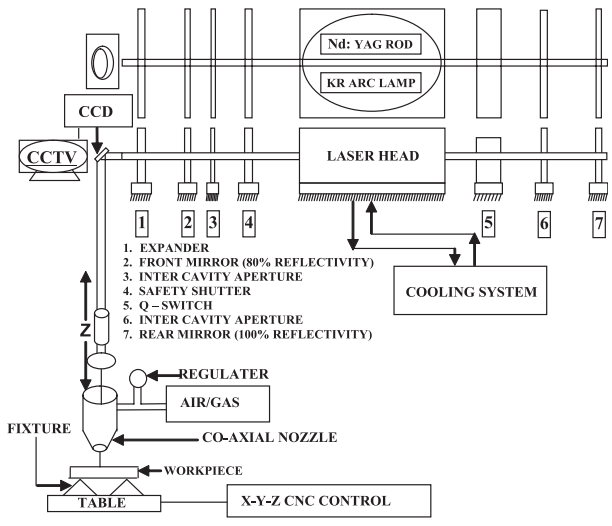

Fig. 1 Schematic representation of the Nd:YAG laser unit

for effective utilization of the energy of the pulsed Nd:YAG laser beam.

3 EXPERIMENTAL DESIGN BASED ON RSM

In the present experimental study, the laser beam microgrooving operation was performed on Al_2TiO_5 of 2.5 mm thickness. Major properties of Al_2TiO_5 are listed in Table 1. Figure 2 is a cross-sectional drawing of the shape of the microgroove to be generated by laser micromachining. The targeted dimensions of the microgroove are upper width of 300 μm, lower width of 100 μm, and depth of 500 μm. The present set of experiments was carried out according to the central composite rotatable second-order design based on RSM [**13**]. The input parameters have predominant impacts on the output criteria of laser micromachining, as the lamp current combined with the pulse frequency provides the energy to remove material and achieve the desired depth. The pulse width provides the accuracy of the microgroove shape. Air pressure is helpful to eject the debris from the narrow gap and at the same time adequate cutting speed is required to generate a good-quality microgroove in sufficient time. Hence, selection of the range of input parameters such as air pressure, lamp current, pulse frequency, pulse width, and cutting speed setting was made after performing some pilot experiments using a fixed focal length.

Table 1 Properties of aluminium titanate (Al_2TiO_5)

Property	Value
Melting temperature (°C)	1860
Decomposition temperature (°C)	1280
Strain rate (s^{-1})	4×10^{-4}
Density (kg/m^3)	3.7×10^3
Specific heat (KJ/kg°C)	650
Thermal expansion coefficient ($°C^{-1}$)	8×10^{-6}
Yield strength (MPa)	11
Effective diffusivity (m^2/s)	6.3×10^{-15}
Modulus of elasticity (GPa)	4
Grain size (μm)	5

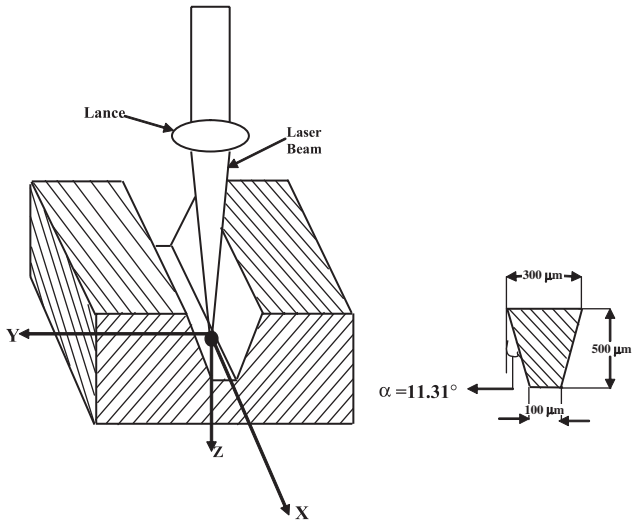

Fig. 2 Cross-sectional drawing of the desired microgroove

Response surface modelling was performed to establish the mathematical relationship between the response, Y_u, and various machining parameters. Equation (1) shows the general second-order polynomial response surface mathematical model for the experimental design

$$Y_u = \beta_0 + \sum_{i=1}^{n} \beta_i X_{iu} + \sum_{i=1}^{n} \beta_{ii} X_{iu}^2 + \sum_{i<j}^{n} \beta_{ij} X_{iu} X_{iu} + e_u \qquad (1)$$

where Y_u is the corresponding response, X_{iu} are coded values of the ith machining process parameters, terms β_0, β_i, β_{ii}, and β_{ij} are the regression coefficients, and e_u the residual experimental error of the uth observation.

Randomized experimental runs were carried out to minimize the error due to machining set-up. The range of air pressure, lamp current, pulse frequency, pulsed width, and cutting speed settings for the experiments are listed in Table 2. Table 3 shows the experimental plan, detailing the experiment run order and coded values of the process parameters. The work sample was mounted on the machining table of the laser machining system with the help of a specially developed workpiece-holding fixture. The response criteria, i.e. the upper width, lower width, and depth in μm of the machined microgrooves, were measured at 10× magnification with the help of an optical measuring microscope (Olympus STM6). Scanning electron micrographs of machined microgrooves were also taken for consideration; Fig. 3 shows a micrograph of the microgrooves machined on a Al_2TiO_5 flat surface. The observed data from the set of experiments were used as inputs to train the ANN predictive model. MINITAB™ Statistical Software Release 13 was used to establish mathematical models for optimization of the laser parameter settings to achieve the required upper width, lower width, and depth condition during pulsed Nd:YAG laser microgrooving on Al_2TiO_5.

Table 2 List of actual and corresponding coded values of the machining process parameters

		Level				
Parameter	Symbol	−2	−1	0	1	2
Air pressure (kg/cm^2)	X_1	0.5	0.9	1.3	1.7	2.1
Lamp current (A)	X_2	15	17	20	22.5	25
Pulse frequency (kHz)	X_3	1	2	3	4	5
Pulse width (%)	X_4	2	4	6	8	10
Cutting speed (mm/s)	X_5	10	14	18	22	26

Table 3 Design of experiments matrix showing coded values and observed responses

	Coded value					Response		
Expt number	X_1	X_2	X_3	X_4	X_5	Upper width (mm)	Lower width (mm)	Depth (mm)
1	−1	−1	−1	−1	1	0.288 875	0.084 50	0.2950
2	1	−1	−1	−1	−1	0.294 250	0.097 37	0.3050
3	−1	1	−1	−1	−1	0.322 750	0.101 256	0.4030
4	1	1	−1	−1	1	0.330 50	0.096 00	0.415 25
5	−1	−1	1	−1	1	0.290 870	0.090 50	0.3567
6	1	−1	1	−1	1	0.290 627	0.0700	0.451 25
7	−1	1	−1	−1	1	0.318 00	0.103 25	0.462 50
8	1	1	1	−1	−1	0.308 70	0.123 45	0.3983
9	−1	−1	−1	1	−1	0.280 50	0.088 75	0.315
10	1	−1	−1	1	1	0.293 00	0.087 00	0.303 75
11	−1	1	−1	1	1	0.320 875	0.110 62	0.513 75
12	1	1	−1	1	−1	0.315 00	0.110 50	0.481 67
13	−1	−1	1	1	1	0.306 125	0.084 25	0.285
14	1	−1	1	1	1	0.291 875	0.088 25	0.2507
15	−1	1	1	1	−1	0.318 35	0.110 125	0.4800
16	1	1	1	1	1	0.320 047	0.119 87	0.491
17	−2	0	0	0	0	0.323 750	0.103 75	0.3583
18	2	0	0	0	0	0.314 50	0.099 00	0.3600
19	0	−2	0	0	0	0.250 00	0.065 00	0.2050
20	0	2	0	0	0	0.331 50	0.129 00	0.511 67
21	0	0	−2	0	0	0.307 50	0.084 50	0.4450
22	0	0	2	0	0	0.314 870	0.100 05	0.416 70
23	0	0	0	−2	0	0.305 50	0.109 125	0.4900
24	0	0	0	2	0	0.301 126	0.106 725	0.435 00
25	0	0	0	0	−2	0.315 245	0.109 050	0.5150
26	0	0	0	0	2	0.307 125	0.102 50	0.4583
27	0	0	0	0	0	0.317 120	0.099 37	0.4300
28	0	0	0	0	0	0.304 50	0.109 90	0.4680
29	0	0	0	0	0	0.304 375	0.098 75	0.4400
30	0	0	0	0	0	0.306 245	0.106 70	0.4910
31	0	0	0	0	0	0.310 625	0.110 00	0.463 67
32	0	0	0	0	0	0.314 675	0.099 80	0.4367

X_1 = air pressure; X_2 = lamp current; X_3 = pulse frequency; X_4 = pulse width; X_5 = cutting speed

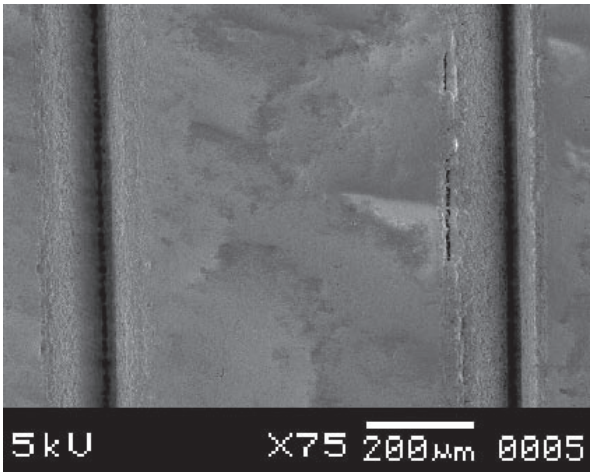

Fig. 3 Scanning electron micrograph of the microgrooves machined on the Al_2TiO_5 flat surface

4 DEVELOPMENT OF ANN MODEL FOR PREDICTION OF RESPONSES

A multilayered neural network computational model can be used for non-linear laser micromachining problems. Among various neural network models, the feedforward neural network based on back-propagation is the best general-purpose model [**14**, **15**]. Using the Matlab Neural Network Toolbox version 6.5 R13, a feedforward neural network was designed based on back-propagation. This is a multilayer architecture made up of one or more hidden layers placed between the input and output layers, where the layers include several processing units known as neurons. These are connected with variable weights to be determined. In the network, each neuron receives total input from all of the neurons in the preceding layer as

$$Y_j = \sum_{j=0}^{N} w_{ij} x_i \tag{2}$$

where Y_j is the total or net input, N is the number of inputs to the jth neuron in the hidden layer, w_{ij} is the weight of the connection from the ith neuron in the forward layer to the jth neuron in the hidden layer, and x_i is the input from the ith neuron in the preceding layer. A neuron in the network produces its output Z_j by processing the net input through an

activation (transfer) function f, such as the tangent hyperbolic function chosen in the present study as

$$Z_j = \mathrm{f}(Y_j) = \frac{1 - \mathrm{e}^{-Y_j}}{1 + \mathrm{e}^{-Y_j}} \tag{3}$$

The optimal neural network architecture used in this study is indicated in Fig. 4. The network consists of one input layer, two hidden layers, and three output layers. Hidden layers have nine neurons each, whereas input and output layers have five and three neurons, respectively. Neurons in the input layer corresponded to air pressure (X_1), lamp current (X_2), pulse frequency (X_3), pulse width (X_4), and cutting speed (X_5). The output layer corresponds to the responses such as upper width, lower width, and depth of the microgroove. To calculate connection weights, a set of desired network output values is needed. Desired output values are sometimes referred to as the training dataset. The training dataset in this study was created with the help of the statistical design of experiments (DOE) method. Upper width, lower width, and depth values corresponding to training data were obtained from experimental runs generated by central composite rotatable second-order design based on RSM. The dataset was generated using the experimental design shown in Table 3. The MATLAB function TRAINGD was utilized for training the data of the network, which works on the back-propagation algorithm. TRAINGD is a network training function that uses the gradient descent method to update the weight variable iteratively and also to minimize the mean square error (MSE) between the predicted data and the training dataset. The change in weight variables is given by

$$\Delta w_{ij} = -\eta \frac{\partial E}{\partial w_{ij}} Z_j \tag{4}$$

where η is the learning rate parameter controlling the rate of convergence and stability of the network model, E is the MSE, and Z_j is the output of the jth neuron. The constant value of learning rate η was chosen as 0.0001. MSE for the training data was calculated as 0.000 099. Figure 5 shows the ANN training of experimentally observed data by MATLAB.

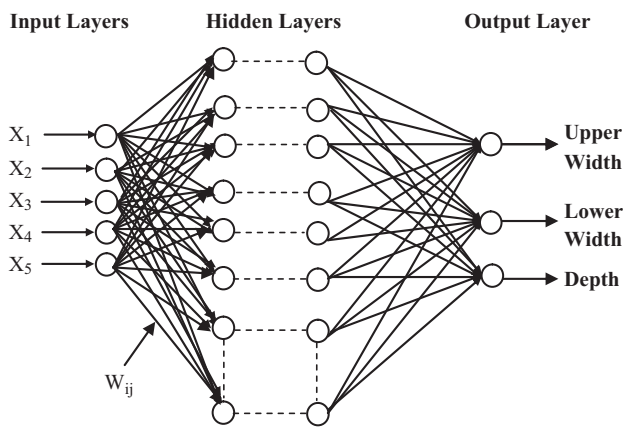

Fig. 4 Neural network architecture designed

4.1 ANN-based results and analysis

The methodology of the ANN-oriented approach is presented in Fig. 6. Training of the neural network model was performed using 29 experimental data points out of 32 as explained in section 3, and Fig. 5 shows the curve generated during the training session. The trained network model was then tested using three experimental data points (check data) which were not used in the training process. The results predicted from the ANN model are compared with those obtained by experiment in Table 4 for three sets of check data and in Table 5 for the 29 training sets. It is seen from Tables 4 and 5 that the ANN prediction is in good agreement with the

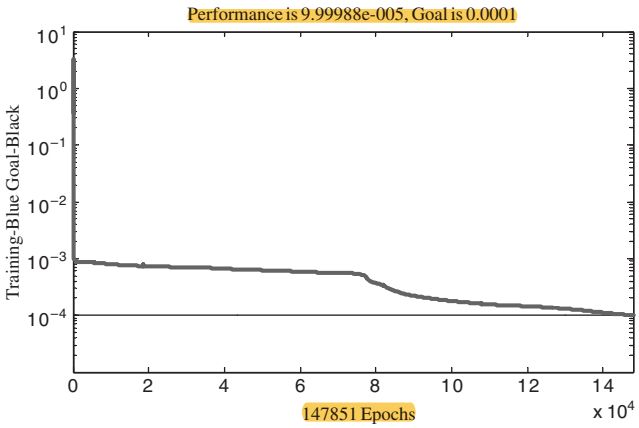

Fig. 5 Generation of curves during a training session

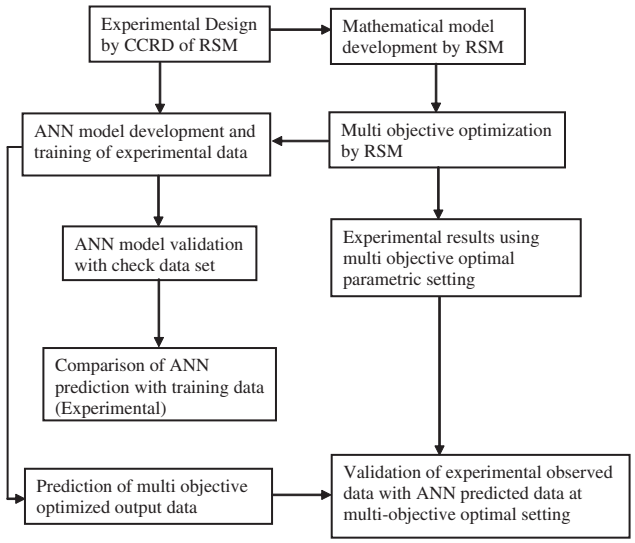

Fig. 6 Methodology of the ANN approach

Table 4 Comparison of ANN prediction with check dataset

	Upper width (mm)		Lower width (mm)		Depth (mm)	
Test number	ANN prediction	Experimental results	ANN prediction	Experimental results	ANN prediction	Experimental results
1	0.2925	0.294 25	0.1076	0.103 25	0.4290	0.415 25
2	0.3218	0.318	0.0966	0.099	0.5100	0.513 75
3	0.3068	0.3075	0.1063	0.106 725	0.4530	0.468 00

Table 5 List of ANN predictions with training datasets

	Upper width (mm)		Lower width (mm)		Depth (mm)	
Test number	ANN prediction	Experimental results	ANN prediction	Experimental results	ANN prediction	Experimental results
1	0.2865	0.288 875	0.0890	0.084 50	0.2950	0.2950
2	0.3171	0.322 750	0.0963	0.097 37	0.3067	0.3050
3	0.3212	0.330 50	0.0927	0.101 256	0.4083	0.4030
4	0.3066	0.290 870	0.1006	0.096 00	0.3585	0.3567
5	0.2979	0.290 627	0.0893	0.090 50	0.4511	0.451 25
6	0.3175	0.308 70	0.0720	0.0700	0.4643	0.462 50
7	0.2752	0.280 50	0.1077	0.123 45	0.4012	0.3983
8	0.3109	0.293 00	0.0907	0.088 75	0.3151	0.3150
9	0.3076	0.320 875	0.0876	0.087 00	0.3037	0.303 75
10	0.3185	0.315 00	0.1058	0.110 62	0.4907	0.481 67
11	0.3088	0.306 125	0.1126	0.110 50	0.2861	0.285
12	0.3095	0.291 875	0.0909	0.084 25	0.2475	0.2507
13	0.3127	0.318 35	0.0993	0.088 25	0.4803	0.4800
14	0.3098	0.320 047	0.1121	0.110 125	0.4958	0.4910
15	0.3120	0.323 750	0.1228	0.119 87	0.3582	0.3583
16	0.3133	0.314 50	0.0928	0.103 75	0.3625	0.3600
17	0.2672	0.250 00	0.0895	0.065 00	0.2066	0.2050
18	0.3253	0.331 50	0.1120	0.129 00	0.5047	0.511 67
19	0.3091	0.314 870	0.0947	0.084 50	0.4357	0.445
20	0.3074	0.305 50	0.0979	0.100 05	0.4140	0.4167
21	0.3089	0.301 126	0.0902	0.109 125	0.4871	0.4900
22	0.3296	0.315 245	0.1065	0.109 05	0.4335	0.4350
23	0.3098	0.307 125	0.0917	0.102 50	0.5184	0.5150
24	0.3132	0.317 120	0.1036	0.099 37	0.4516	0.4583
25	0.3132	0.304 50	0.1036	0.109 90	0.4516	0.4300
26	0.3132	0.304 375	0.1036	0.098 75	0.4516	0.4680
27	0.3132	0.306 245	0.1036	0.106 70	0.4516	0.4400
28	0.3132	0.310 625	0.1036	0.110 00	0.4516	0.4910
29	0.3132	0.314 675	0.1036	0.099 80	0.4516	0.463 67

experimental results. Figures 7 and 8 compare the neural network prediction results for upper width with the experimental test results for the check and training datasets, respectively; Figs 9 and 10 present comparisons for the lower width, and Figs 11 and 12 for the depth. It is found that the developed ANN model has good interpolation capability and can be used as an efficient predictive tool for laser micro-grooving parameters.

5 OPTIMIZATION OF RESPONSES USING RSM

Mathematical models based on RSM for correlating responses such as the upper width, Y_U, lower width, Y_L, and depth, Y_D, of the microgroove with various settings of the predominant laser machining process parameters as considered in the experimental design have been established, and are represented in the following regression equations

$$\begin{aligned} Y_U = {} & 0.30994 - 0.00290X_1 - 0.03214X_2 - 0.00148X_3 \\ & + 0.000694X_4 + 0.00378X_5 + 0.00815X_1^2 - 0.02027X_2^2 \\ & + 0.00027X_3^2 - 0.00760X_4^2 + 0.00027X_5^2 - 0.00220X_1X_2 \\ & - 0.00942X_1X_3 + 0.00158X_1X_4 + 0.00469X_1X_5 \\ & - 0.01568X_2X_3 - 0.00418X_2X_4 - 0.00017X_2X_5 \\ & + 0.01276X_3X_4 + 0.00002X_3X_5 + 0.00176X_4X_5 \end{aligned} \quad (5)$$

$$\begin{aligned} Y_L = {} & 0.10448 + 0.00091X_1 + 0.02615X_2 + 0.00373X_3 \\ & + 0.00235X_4 - 0.00565X_5 - 0.00430X_1^2 - 0.00897X_2^2 \\ & - 0.01336X_3^2 + 0.00229X_4^2 + 0.00014X_5^2 + 0.00686X_1X_2 \\ & + 0.00193X_1X_3 + 0.00114X_1X_4 - 0.00967X_1X_5 \\ & + 0.01573X_2X_3 + 0.00532X_2X_4 + 0.00588X_2X_5 \\ & - 0.00061X_3X_4 - 0.00380X_3X_5 + 0.01574X_4X_5 \end{aligned} \quad (6)$$

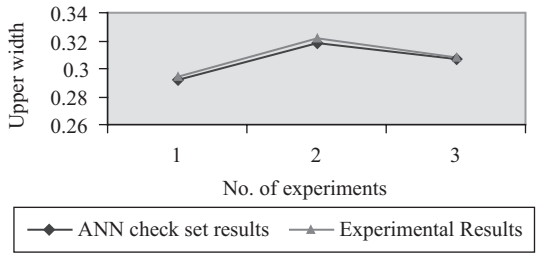

Fig. 7 Comparison of ANN predictions with the check dataset for the upper width of the microgroove

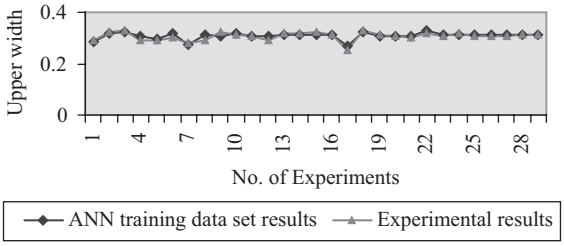

Fig. 8 Comparison of ANN predictions with the training dataset for the upper width of the microgroove

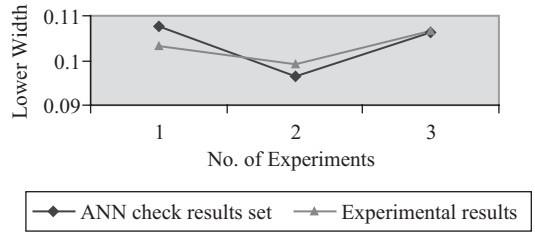

Fig. 9 Comparison of ANN predictions with the check dataset for the lower width of the microgroove

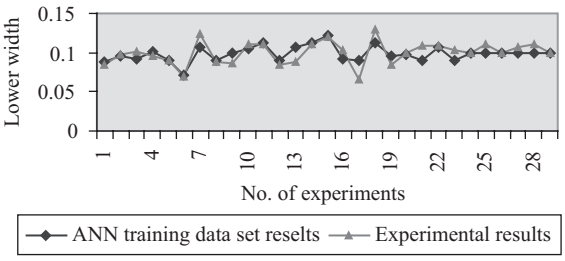

Fig. 10 Comparison of ANN predictions with the training dataset for the lower width of the microgroove

$$
\begin{aligned}
Y_{\mathrm{D}} = {} & 0.4591 - 0.0009X_1 + 0.1404X_2 + 0.0072X_3 \\
& - 0.0063X_4 + 0.0095X_5 - 0.1127X_1^2 - 0.1107X_2^2 \\
& - 0.0410X_3^2 - 0.0094X_4^2 + 0.0148X_5^2 - 0.0327X_1X_2 \\
& + 0.007X_1X_3 - 0.0298X_1X_4 + 0.0560X_1X_5 \\
& - 0.00267X_2X_3 + 0.1352X_2X_4 + 0.0030X_2X_5 \\
& - 0.0895X_3X_4 + 0.0452X_3X_5 - 0.0237X_4X_5 \qquad (7)
\end{aligned}
$$

Optimization analyses of the individual responses were performed separately for achieving the desired upper

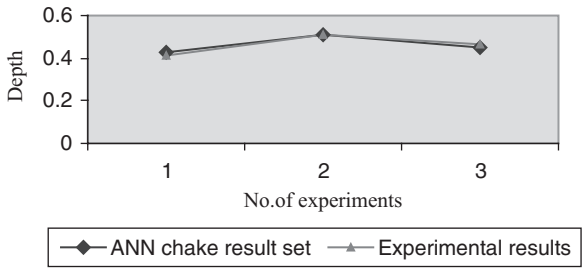

Fig. 11 Comparison of ANN predictions with the check dataset for the depth of the microgroove

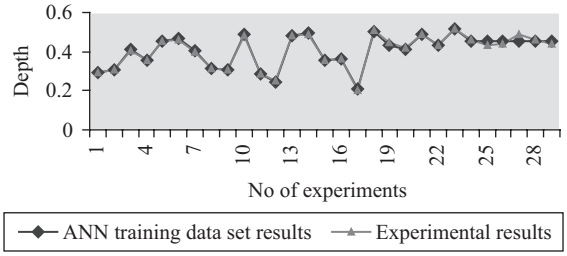

Fig. 12 Comparison of ANN predictions with the training dataset for the depth of the microgroove

width, lower width, and depth based on the developed mathematical models, i.e. equations (5), (6), and (7). The MINITAB software was used to optimize the responses during laser microgrooving on Al_2TiO_5 and the target values for the upper width, lower width, and depth of the microgroove were set as 300 μm, 100 μm and 500 μm, respectively. Optimization results for achieving the required or targeted upper width, lower width, and depth during the microgrooving operation on Al_2TiO_5 are shown in Figs 13 to 15, respectively. In these figures, each column of the plot corresponds to a factor and each row of the plot corresponds to a response, where each cell of the plot shows how one of the responses changes as a function of one of the factors with all other factors remaining fixed. The numbers displayed at the top of a column show the current factor settings and the high and low settings of the factor in the experimental design. At the left of each row, the goal for the response (i.e. the targeted response), the response, *y*, at current factor settings, and the individual desirability score, *d*, are given. The optimal response plots were generated using MINITAB software. The vertical lines inside the cells represent current optimal parametric settings, and the horizontal dotted lines represent the current response values. Calculated individual RSM optimal parameters are listed in Table 6. The current optimal parameter settings for achieving the desired upper width are air pressure of 0.50 kgf/cm^2, lamp current of 15.27 A, pulse frequency of 4.8 kHz, pulse width of 10 per cent of duty cycle, and cutting speed of 10 mm/s. The optimal parametric settings for lower width of the microgroove are air pressure of 1.96 kgf/cm^2, lamp current

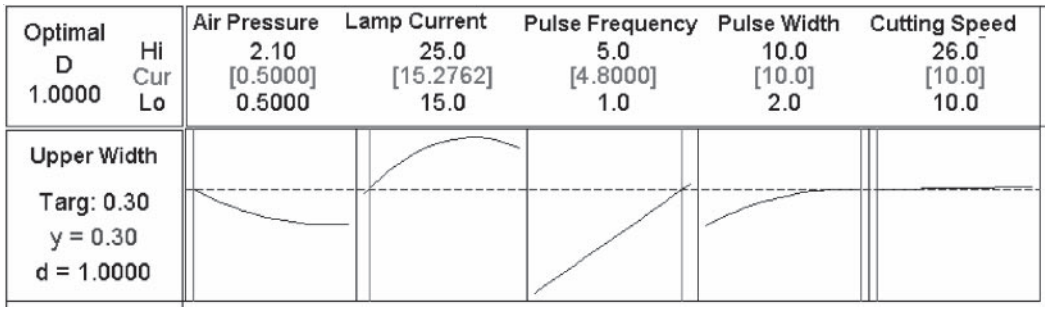

Fig. 13 Optimization results for the upper width of the microgroove

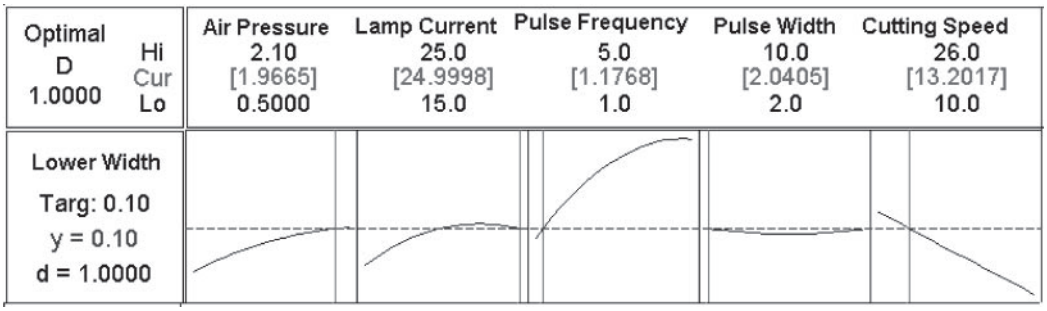

Fig. 14 Optimization results for the lower width of the microgroove

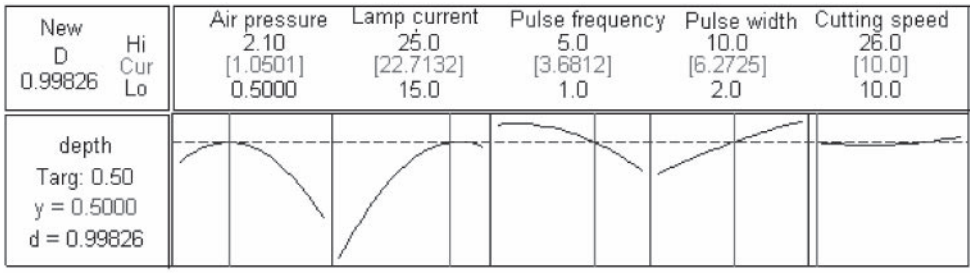

Fig. 15 Optimization results for the depth of the microgroove

of 24.99 A, pulse frequency of 1.27 kHz, pulse width of 2.04 per cent of duty cycle, and cutting speed of 13.2 mm/s. The optimal parametric settings for depth are air pressure of 1.0501 kgf/cm^2, lamp current of 22.7132 A, pulse frequency of 3.6812 kHz, pulse width of 6.2725 per cent of duty cycle, and cutting speed of 10 mm/s. The ANN model was used to predict the output of optimal individual input settings as obtained by RSM model optimization; the outputs of the ANN model are shown in Table 7. The predicted individual results of the ANN model show a very good agreement with the targeted output of upper width, lower width, and depth of the laser microgroove operation.

6 MULTI-OBJECTIVE PARAMETRIC OPTIMIZATION OF THE MICROGROOVE

Multi-objective optimization analysis was performed to achieve the target value of all three responses, i.e. upper width, lower width, and depth of the laser microgroove based on the developed mathematical equations (5), (6), and (7) for the Al_2TiO_5 ceramic material. The MINITAB software was also utilized for multi-objective optimization. Upper width, lower width, and depth were targeted together in one setting. The multi-objective optimum parametric settings obtained are represented in Fig. 16 and the optimization results are given in Table 6.

The current optimal process parameter settings are air pressure of 1.2944 kgf/cm^2, lamp current of 19.3070 A, pulse frequency of 1.755 kHz, pulse width of 5.7087 per cent of duty cycle, and cutting speed of 10 mm/s for achieving the targeted upper width Y_U of 0.3 mm, lower width Y_L of 0.1 mm, and depth Y_D of 0.5 mm. The value of composite desirability, D, was taken as 1. All three responses are optimized at the above parametric combination with D of 0.93127 and optimized response values of Y_U, Y_L, and Y_D are 0.3 mm, 0.0997 mm, and 0.4451 mm,

Table 6 List of RSM optimal parameter settings for the upper width, lower width, and depth of the microgroove

Parameter	Optimal parameter setting for upper width (300 μm)	Optimal parameter setting for lower width (100 μm)	Optimal parameter setting for depth (500 μm)	Multi-objective optimal parameter setting for upper, lower width, and depth (300 μm, 100 μm, 500 μm)
Air pressure	0.5	1.9665	1.0501	1.2944
Lamp current	15.2762	24.9998	22.7132	19.3070
Pulse frequency	4.8	1.1768	3.6812	1.755
Pulse width	10	2.0405	6.2725	5.7087
Cutting speed	10	13.2017	10	10

Table 7 List of ANN-predicted outputs of RSM optimal parameter setting inputs

	ANN outputs			Experimental outputs			Percentage error		
Optimal settings	Upper width	Lower width	Depth	Upper width	Lower width	Depth	Upper width	Lower width	Depth
Individual optimal	0.3054	0.1039	0.5079	–	–	–	–	–	–
Multi-objective optimal	0.3026	0.0993	0.4789	0.301 16	0.1005	0.4965	0.5	1.2	3.52

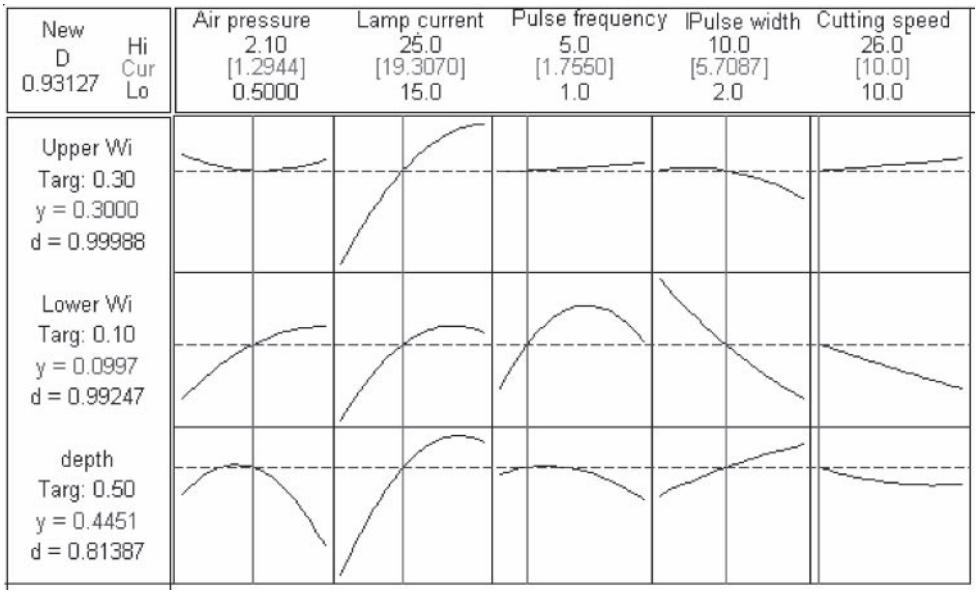

Fig. 16 Multi-objective optimization results for the upper width, lower width, and depth of the microgroove

respectively. An experiment was carried out to cut the microgroove at the above optimal parametric settings for upper width, lower width, and depth. Observed dimensions of the machined microgroove on Al_2TiO_5 were 0.301126 mm, 0.1005 mm, and 0.4965 mm for upper width, lower width, and depth respectively. The outputs of the ANN prediction to the optimal input parameter setting based on multi-objective optimization are 0.3026 mm, 0.1005 mm, and 0.4789 mm, respectively. Table 7 shows the ANN prediction and experimental results with the multi-objective parametric optimal setting as obtained from the RSM model. Predictions are in good agreement with the measured experimental values. The percentage error of the predicted value with respect to the experimentally observed value of upper width, lower width, and depth is within 5 per cent, which is acceptable.

From the optimization results it is found that, at moderately high lamp current, low frequency, and medium pulse width, the desired microgroove geometry can be achieved. As the lamp current is high and the frequency is low, the beam power is high which evaporates the material at a faster rate and as a result the penetration depth is high. At the same time the desired shape is generated by virtue of the medium pulse width because sufficient peak power is reached to evaporate the material from the desired

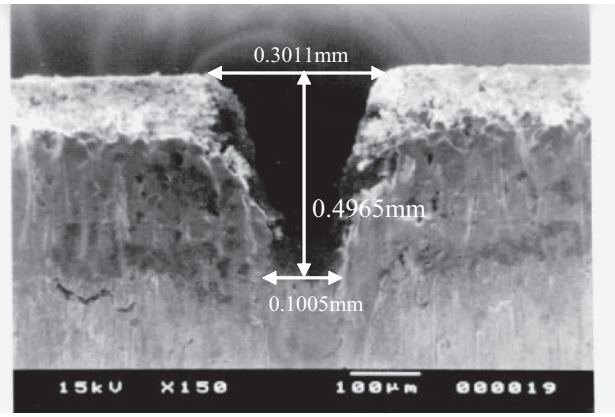

Fig. 17 Scanning electron micrograph showing the cross-section of the microgroove cut at optimal multi-objective parametric settings for upper width, lower width, and depth

area of the microgroove. Air pressure and cutting speed also play a vital role: the moderately high air pressure results in molten material being removed from the microgroove and helps to protect the microgroove boundary from the generation of a HAZ by taking away the heat energy along with the flow of air. For a good-quality microgroove, low cutting speed is recommended because sufficient time is available to melt and remove material from the desired area of the microgroove. Figure 17 is a scanning electron micrograph of the microgroove machined at the multi-objective optimal parametric setting for upper width, lower width, and depth during laser microgroove operation on Al_2TiO_5.

7 CONCLUSIONS

In the current study, experimental observations of a Nd:YAG laser machining system have been incorporated into an ANN model for predicting parameter settings to achieve precision microgrooving operations on Al_2TiO_5. A multilayered feedforward neural network was combined with the results of RSM optimization to enable prediction of the desired upper width, lower width, and depth of laser microgrooves. From the experimental investigation, RSM, and ANN model development for machining of Al_2TiO_5 by Nd:YAG laser, the following conclusions can be drawn.

1. For examining experimental data and ANN predictive data on microgroove width and depth phenomena, the developed models are adequate for determining the upper width, lower width, and depth for setting the optimal Nd:YAG laser machining parameters within the selected input range during laser microgrooving operations. These models can be utilized to achieve precise dimensions of microgrooves on Al_2TiO_5.
2. The ANN model predicts optimum individual response values, i.e. upper width, lower width, and depth, that are close to the target dimensions of the microgroove by using optimum input parameters based on RSM during laser machining operation.
3. As per the result obtained during mathematical modelling of optimization, the individual optimizations of input parameters are more effective than the multi-objective optimized input parameters.
4. From the multi-objective optimization, the optimal combination of parameter settings is air pressure of 1.2944 kgf/cm^2, lamp current of 19.3070 A, pulse frequency of 1.755 kHz, pulse width of 5.7087 per cent of duty cycle, and cutting speed of 10 mm/s for achieving the required upper width, lower width, and depth.
5. In analysing the ANN-predicted outputs and experimentally observed outputs for multi-objective optimal input process parametric settings as obtained through RSM model optimization, it is found that the percentage of error is within 5 per cent, which is acceptable. Moreover, the ANN-predicted outputs have been validated through experimentation.
6. The advantage of optimization techniques as applied in the present work is that they provide the mathematical relationships between responses and machining process parameters to determine the optimal combinations of input parameters. The developed ANN model can be used as a knowledge base to generate the predicted optimal outputs.

The ANN model can also be used for seeking the optimal parameter settings for different desired geometry of grooves for Al_2TiO_5 material. The outcome of the present research based on RSM and ANN models in the area of the pulsed Nd:YAG laser micromachining of engineering ceramics can be effectively utilized for the investigation and prediction of optimal Nd:YAG laser process parametric settings for micromachining and microfabrication of different ceramic materials with intricate shape geometries.

ACKNOWLEDGEMENTS

The authors acknowledge the financial support from the Department of Science and Technology (DST), New Delhi, under the scheme of DST SERC Fast Track Project and also from the University Grants Commission (UGC), New Delhi, under the CAS Ph-III programme.

REFERENCES

1 **Tilloca, G.** Thermal stabilization of aluminum titanate and properties of aluminum titanate solid solutions. *J. Mater. Sci.*, 1991, **26**, 2809–2814.

2 **Chryssolouris, G.** *Laser machining: theory and practice*, 1991, pp. 209–265 (Springer-Verlag, New York).
3 **Choi, W. C.** and **Chryssolouris, G.** Analysis of the laser grooving and cutting processes. *J Phys. D: Appl. Phys.*, 1995, **28**, 863–878.
4 **Kuar, A. S., Doloi, B.,** and **Bhattacharyya, B.** Modeling and analysis of pulsed Nd:YAG laser machining characteristics during micro-drilling of zirconia (ZrO_2). *Int. J. Machine Tools Mf.*, 2006, **46**, 1301–1310.
5 **Engin, D.** and **Kirby, K. W.** Development of analytical model for the laser machining of ceramic and glass–ceramic materials. *J. Appl. Phys.*, 1996, **80**, 681–690.
6 **Mai, C. C.** and **Lin, J.** Supersonic flow characteristics in laser grooving. *Optics Laser Technol.*, 2003, **35**, 597–604.
7 **Farooq, K.** and **Kar, A.** Removal of laser-melted material with an assist gas. *J. Appl. Phys.*, 1998, **83**(12), 7467–7473.
8 **Black, I., Livingstone, S. A. J.,** and **Chua, K. L.** A laser beam machining (LBM) database for the cutting of ceramic tile. *J. Mater. Process. Technol.*, 1998, **84**, 47–45.
9 **Lallemanda, G.** Grooving by Nd:YAG laser treatment. *J. Mater. Process. Technol.*, 2000, **99**, 32–37.
10 **Tuersley, I. P., Hoult, A. P.,** and **Pashby, I. R.** The processing of magnesium-alumino-silicate matrix, SiC fiber glass–ceramic matrix composite using a pulsed Nd:YAG laser. *J. Mater. Sci.*, 1996, **31**, 4111–4119.
11 **Booth, J.** Recent application of pulsed lasers in advanced materials processing. *Thin Solid Films*, 2004, **453–454**, 450–457.
12 **Yousef, B. F., Knopf, G. K., Bordatchev, E. V.,** and **Nikumb, S. K.** Neural network modeling and analysis of the material removal process during laser machining. *Int. J. Adv. Mfg Technol.*, 2003, **22**, 41–53.
13 **Montgomery, D. D.** Design and analysis of experiments, fifth edition, 2001, pp. 427–500 (John Wiley & Sons, New York).
14 **Haykin, S.** *Neural networks: a comprehensive foundation*, 2002, pp. 178–193 (Pearson, Harlow).
15 **Hassoun, M. H.** *Fundamentals of artificial neural networks*, 1995, pp. 197–233 (MIT Press, Cambridge, MA).

APPENDIX

Notation

e_u	residual error
E	mean square error
f	activation function
N	number of inputs
w_{ij}	weight of connection
x_i	input from the ith neuron
X_{iu}	coded value of machining processes
Y_D	depth of the microgroove
Y_j	net input
Y_L	lower width of the microgroove
Y_u	corresponding response
Y_U	upper width of the microgroove
Z_j	output of the jth neuron
β	regression coefficient
η	learning rate